TABLE II: Intrinsic Dimension D of Some Simple Two-Dimensional Clusters Defined by the Relationship of Cluster Mass M to Radial Extent R; i.e., log M = D log R[a]

radial line	$y = ax$	$D = 1$
equiangular spiral	$\log r = a\theta$	$D = 1$
Archimedes spiral	$r = a\theta$	$D = 2$
power-law signal	$\log r = a \log \theta$	$D = 1 + a$

[a] In each case, we have assumed that a simple curve having some given constant width defines the elementary topology of a two-dimensional cluster.

of a straight line is unity (Table II), this suggest that the branching multiplicity goes as the radial distance to the 0.7 power.

We close by noting that the presently popular parameter *fractal dimension* tells us little about the true visual richness of form in even the most simplistic of cases. We further illustrate this conclusion by the following example. We assume that a simple curve having some given constant width defines the elementary topology of a two-dimensional cluster, and we calculate its *intrinsic*

dimension defined by the relationship of cluster mass M to radial extent R; i.e., log $(M) = D$ log (R) (Table II). We note that this *intrinsic* dimension would not distinguished between radially diverging straight lines and the equiangular spiral (intrinsic dimension equal to unity) or between an Archimedian spiral and a solid circle (intrinsic dimension equal to two). Also, it seems strange to presuppose that examples having the same fractal dimension would have much in common concerning their form (as well as their growth). And yet, such practice is adopted in current literature. A similar conclusion has been reached by Hoover.[30] He states: "It is clear that the fractal dimensionality is a far-from-complete description of geometry. Both a smooth two-dimensional surface and a Brownian trajectory in three-dimensional space have the *same* fractal dimensionality, but they are very different from the geometric point of view."

(30) Hoover, W. G. *Molecular Dynamics*; Springer-Verlag: Berlin, 1986; Lecture Notes in Physics No. 258, p 108.

Electron Excitation Dynamics, Localization, and Solvation in Small Clusters

Uzi Landman,* R. N. Barnett, C. L. Cleveland,

School of Physics, Georgia Institute of Technology, Atlanta, Georgia 30332

Dafna Scharf, and Joshua Jortner

School of Chemistry, Tel Aviv University, 69978 Tel Aviv, Israel (Received: December 2, 1986)

The energetics and dynamics of electronically excited rare-gas clusters and modes of electron attachment and solvation in alkali halide clusters and in water clusters are investigated by classical and quantum path-integral molecular dynamics techniques. We demonstrate the versatility and degree of spatial and temporal detail afforded by computer simulations and the new avenues which such studies open for studies of physical and chemical phenomena, not accessible by other modes of investigation.

1. Introduction

Structural, electronic, dynamic, and chemical characteristics of materials depend primarily on the state (phase) and degree (size) of aggregation. Small clusters often exhibit unique physical and chemical phenomena, of both fundamental and technological significance, and provide the opportunity for exploration of the transition from molecular to condensed matter systems. Particularly, investigations of the correlations between physical properties and degree of aggregation allow elucidation of the development of collective phenomena responsible for phase transformations[1,2] (such as nucleation, melting, and structural transitions), studies of the excitation dynamics and the kinetics of reactive processes[3,4] (such as fragmentation) and of the energetics and dynamics of electron attachment,[5,6] solvation phenomena,[7] and physical processes induced by electron attachment.

In this paper we focus on the energetics and dynamics of electronically excited clusters and on electron attachment and solvation in clusters. Theoretical studies of clusters were hampered by the relatively large number of particles which renders the adaptation of molecular science techniques rather cumbersome, while the lack of translational symmetry prevents the employment of solid-state methodology. These problems are alleviated by computer simulations,[8,9] where the evolution of the system is simulated, with refined temporal and spatial resolution, via direct numerical solution of the equations of motion and are in a sense computer experiments which open new avenues in investigations of the microscopic origins of physical phenomena. We demonstrate the versatility and wealth of information obtained from computer simulations via classical molecular dynamics (MD) as well as quantum path-integral molecular dynamics (QUPID) calculations. The dynamics of electronically excited clusters and vibrational predissociation phenomena induced by excitation of inert-gas clusters[3] are discussed in section 2. The QUPID method and its applications to studies of electron attachment and localization in alkali halide clusters[5] and of cluster isomerization induced by electron attachment are described in section 3. Electron at-

(1) Jellinek, J.; Beck, T. L.; Berry, R. S. *J. Chem. Phys.* **1983**, *84*, 2783, and references therein.
(2) Luo, J.; Landman, U.; Jortner, J. *Proceedings of the International Conference on the Physics and Chemistry of Small Clusters*, Richmond, VA, Nov, 1986; Plenum: New York, in press.
(3) Scharf, D.; Jortner, J.; Landman, U. *Chem. Phys. Lett.* **1986**, *126*, 495.
(4) Jortner, J. *Ber. Bunsen-Ges. Phys. Chem.* **1984**, *88*, 188.
(5) Landman, U.; Scharf, D.; Jortner, J. *Phys. Rev. Lett.* **1985**, *54*, 1860.
(6) Mark, T. D.; Castleman, Jr., A. W. *Adv. At. Mol. Phys.* **1984**, *20*.
(7) See papers in *J. Phys. Chem.* **1984**, *88*.

(8) Abraham, F. F. *J. Vac. Sci. Technol.* **1984**, *B2*, 534.
(9) Landman, U.; et al. *Mat. Res. Soc. Symp. Proc.* **1985**, *63*, 273.

tachment to water clusters is discussed in section 4.

Throughout our investigations, the seminal contributions of Aneesur Rahman to the development and implementation of the methodology and practice of computer simulations are clearly evidenced. Having been touched and influenced by Rahman's work for many years, we dedicate this paper to him with gratitude and deep appreciation.

2. Dynamics of Electronically Excited Clusters

The processes of energy acquisition, storage, and disposal in clusters are of considerable interest for the elucidation of dynamic processes in finite systems, whose energy spectrum for electronic and nuclear excitations can be varied continuously by changing the cluster size.[10] In this context, an important issue involves the consequences of vibrational excitations of clusters. Such relaxation processes fall into two categories: (1) Nonreactive vibrational energy redistribution in the cluster, which does not result in dissociation, and (2) reactive dissociation or vibrational predissociation. The mechanisms of vibrational energy acquisition by a cluster can involve collisional excitation, optical photoselective vibrational excitation, or electronic excitation followed by the degradation of electronic energy into vibrational energy. In charged clusters, the vibrational excitation resulting in both nonreactive and reactive relaxation can originate from ionization followed by hole trapping in inert-gas clusters[11] and from electron attachment to alkali halide clusters.[5,6] In neutral clusters, it was found, using MD simulations,[12] that the dissociation of Ar_n (n = 4–6) clusters can be accounted for in terms of the statistical theory of unimolecular reactions, which implies the occurrence of vibrational energy randomization in small clusters. The non-reactive and reactive processes induced by the degradation of electronic energy into vibrational energy in clusters have not yet been elucidated. An interesting problem in this category involves the dynamical consequences of exciton trapping in rare-gas clusters (RGCs), which is the focus of our study. Extensive information is currently available regarding exciton trapping in solid and liquid inert gases.[13] Exciton trapping in the heavy rare-gas solids, i.e., Ar, Kr, and Xe, exhibits two-center localization, resulting in the formation of electronically excited, diatomic inert-gas excimer molecules. Electronic excitation of a RGC, R_n, is expected to result in an exciton state, which subsequently becomes trapped by self-localization. Although the details of the energetics and spatial charge distribution of excitons in finite RGCs have not yet been explored, some information can be drawn from the analogy with the lowest electronic excitation in solid and liquid rare gases.[13] The two lowest, dipole-allowed, electronic excitations in RGCs can adequately be described in terms of tightly bound, Frenkel-type excitations with a parentage in the $^1S_1 \rightarrow {}^3P_1$ and $^1S_0 \rightarrow {}^1P_1$ atomic excitations which are modified by large nonorthogonality corrections.[13] The process of exciton trapping in the heavy RGCs of Ar, Kr, and Xe involves the formation of the diatomic excimer molecule R_2^*, which is characterized by a substantial binding energy at a highly vibrational state. Energy exchange between the R_2^* excimer and the cluster in which it is embedded involves two processes.

(1) Short-range repulsive interactions between the expanded, Rydberg-type excited state of the excimer and the other cluster atoms result in a dilation of the local structure around the excimer, leading to energy flow into the cluster.

(2) Vibrational relaxation of the excimer induces vibrational energy flow into the cluster.

The vibrational energy released into the cluster by processes 1 and 2 may result in vibrational predissociation.

We have explored the dynamic implications of exciton trapping in RGCs by conducting classical molecular dynamics (MD)

calculations[8,9] on electronically excited states of such clusters. As model systems we have chosen, Ar_n (with n = 13, 55) and mixed $Xe_m Ar_{n-m}$ (m = 1, 2 and n = 13, 55) clusters. The ground states of the RGCs were described by Lennard-Jones pair potentials $V(r)$ = $4\epsilon[(\sigma/r)^{12} - (\sigma/r)^6]$ with the well-depth and distance parameters appropriate for Ar–Ar[14] (121 K, 3.4 Å), Ar – Xe[15] (177.6 K, 3.65 Å), and Xe–Xe[16] (222.3 K, 4.10 Å). In the electronically excited state the excimer potential is represented by a Morse curve, $V(r)$ = $D_e\{\exp(-2B(r/R_e - 1)] - 2 \exp[-B(r/R_e - 1)]\}$ with the parameters D_e, R_e, and B taken as 9125.3 K, 2.319 Å, and 5.12 for Ar_2^*[17] and 11609 K, 2.99 Å, and 4.228 for Xe_2^*.

An important consequence of the electronic excitation involves the drastic modification of the interaction between the excimer and the ground-state atoms. On the basis of the analysis of Xe^*–Ar interactions[15] (for which a description in terms of a 6–12 LJ potential with ϵ = 92.8 K and σ = 4.13 Å is adequate) the Ar^*–Ar potential for each of the constituents of the excimer has been described in terms of a Lennard-Jones potential with the parameters ϵ^* and σ^*. We have taken for the energy $\epsilon^* = \epsilon$, while the distance scale ratio $\bar{\sigma} = \sigma^*/\sigma$ has been chosen in the range $\bar{\sigma}$ = 1.0–1.2. The apprpriate Ar^*–Ar interaction is characterized by[15] $\bar{\sigma}$ = 1.10–1.15, reflecting the enhancement of short-range repulsive interactions in the electronically excited Rydberg-type state.

Following equilibration of the ground-state system, electronic excitation was achieved (at the time t = 0) by the instantaneous switching on of the excimer potential between a pair of nearest-neighbor atoms and of the potentials between the excimer and the ground-state atoms comprising the rest of the cluster (using a fifth-order predictor–corrector method, the integration time step in the ground state was 1.6×10^{-14} s and in the excited state 1.6×10^{-16} s).

We consider first the dynamics of excited homonuclear clusters, Ar_{13}^* and Ar_{55}^*. In Figure 1, a and b, we show an overview of the dynamics of the nuclear motion following the electronic excitations in Ar_{13}^* which is expressed in terms of the interatomic distances. The excimer exhibits a large amplitude motion in a highly excited vibrational state, while all the other interatomic distances increase, indicating the initiation of the escape of the ground-state cluster atoms. Insight into the energy flow from the excimer into the cluster is obtained from the time dependence of the kinetic energy (KE), the potential energy (PE), and the total energy of the excimer (Figure 2). The strong oscillations in the PE and KE clearly indicate the persistence of the vibrational excitation of the excimer over a long time scale. Further detailed information concerning the implications of this energy flow on the cluster dissociation was inferred by considering the composition and the energetics of the "main fragment", i.e., the fragment which consists of the excimer together with ground-state atoms, with all the nearest-neighbor separations being smaller than 3σ, beyond which all interatomic interactions are negligibly small. The total energy within the main fragment was partitioned into two separate contributions: (1) The energy of the "reaction center", which consists of the excimer PE and KE together with half of the sum of the potential energy of the Ar^*–Ar interactions, and (2) the energy of the "bath subsystem", which involves the KE of the ground-state Ar atoms, the potential energies of the Ar–Ar interactions, and half of the sum of the potential energies of the Ar^*–Ar interactions. The time evolution of the various contributions to the total energy (Figure 3) portrays the energy flow from the excitation center into the "bath". However, the energy per atom does not equilibrate. Discontinuities (i.e., "steps") in the energy plots of Figure 3 mark the dissociation of the main fragment, with the decrease of the total energy corresponding to the KE of the ground-state atoms dissociating from it. A cursory examination of the time evolution of the composition of the main

(10) See papers in *Ber. Bunsen-Ges. Phys. Chem.* **1984**, *88*, 188.

(11) Haberland, H. *Surf. Sci.* **1985**, *156*, 305. Saenz, J. J.; Soler, J. M.; Garcia, N. Ibid. **1985**, *156*, 121.

(12) Brady, J. W.; Doll, J. D. *J. Chem. Phys.* **1980**, *73*, 2767.

(13) Jortner, J.; Koch, E. E.; Schwentner, N. In *Photo-Physics and PhotoChemistry in the Vacuum UV*, McGlynn, S. P., et al., Eds.; Reidel: Dordrecht, 1985; p 515.

(14) Kristensen, W. D.; Jensen, E. J.; Cotterill, M. J. *J. Chem. Phys.* **1974**, *60*, 4161.

(15) Messing, I.; Raz, B.; Jortner, J. *J. Chem. Phys.* **1977**, *66*, 2239.

(16) Sherwood, A. E.; Prasunitz, J. M. *J. Chem. Phys.* **1964**, *41*, 429.

(17) Gillen, K. T.; Saxon, R. P.; Lorentz, D. C.; Ice, G. E.; Olson, R. E. *J. Chem. Phys.* **1975**, *64*, 1925.
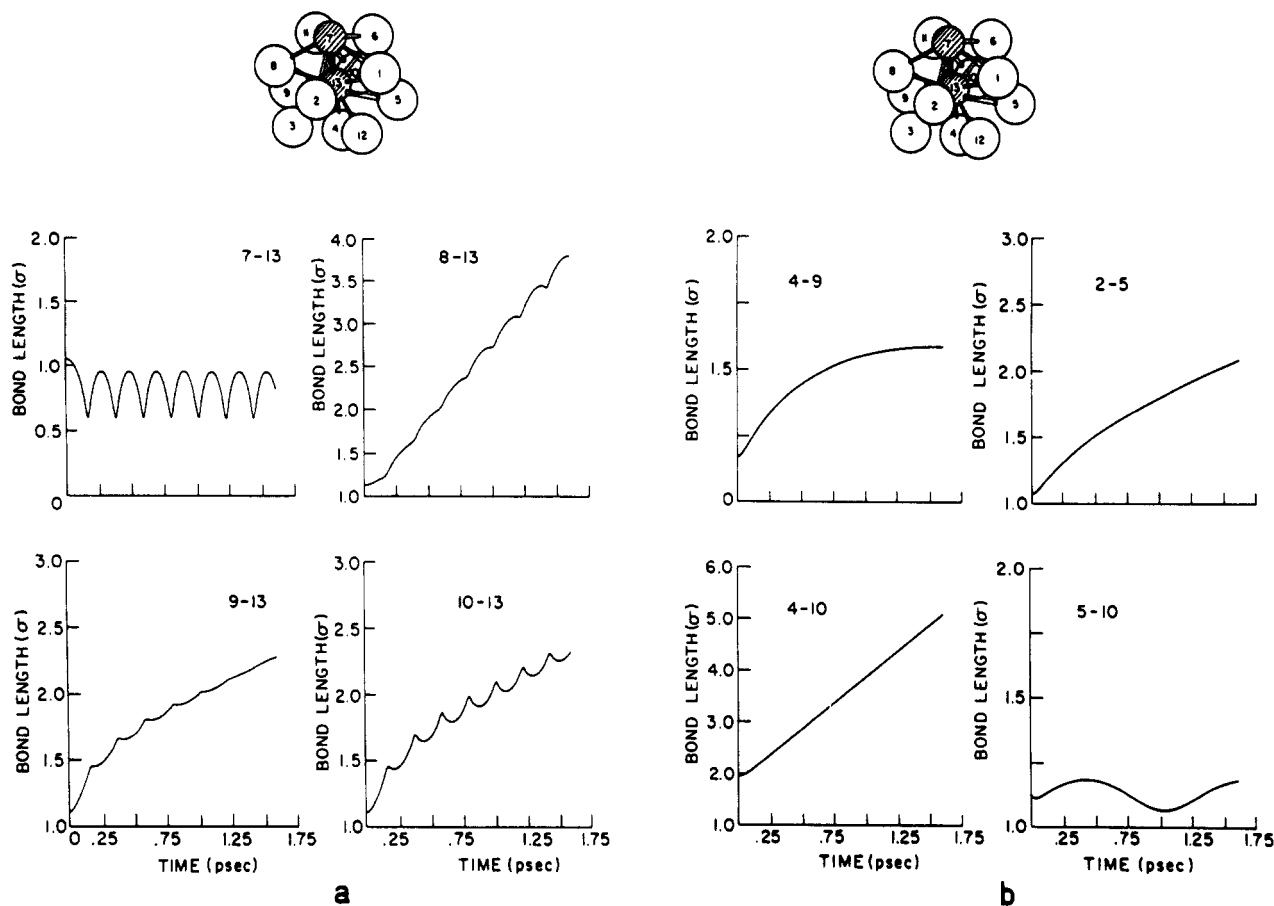
Figure 1. Time dependence of interatomic distances in the electronically excited Ar_{13}^* cluster. The insert shows the ground-state equilibrium structure at 24 K. The labeling of atoms is indicated. The dashed atoms 7 and 13 form the excimer. Distances are in units of σ. The Ar^*–Ar interaction is characterized by $\bar{\sigma} = 1.20$. (a) Interatomic distances within the excimer and between the excimer atoms and some ground-state atoms. (b) Interatomic distances between some ground-state atoms.

fragment (Figure 3) clearly indicates that the major fragmentation process involves the sequential stepwise dissociation, i.e., "evaporation", of single ground-state atoms from the main fragment. The escape of the excimer from the main fragment has not been encountered. The dissociation process is dominated by the magnitude of the excited-state potential scale parameter $\bar{\sigma}$. For realistic values[15] of $\bar{\sigma} = 1.10–1.20$, the threshold for cluster dissociation is exhibited on the time scale of $\sim$2–20 ps (Figure 4).

From these MD results the following picture concerning vibrational energy flow and reactive dynamics of the Ar_{13} cluster emerges. The temporal persistence of the vibrational excitation of the excimer (Figure 2) and of the "reaction center" (Figure 3) corresponds to a "mode selective" excitation of the excimer, with vibrational energy redistribution within the cluster being precluded by two effects: first, the difference in the characteristic frequencies of the (high frequency) excimer motion and the (low frequency) motions of the cluster; second, the local dilation of the cluster structure around the excimer, which is induced by the short-range excimer–cluster repulsive interactions. The vibrational energy flow from the dimer into the cluster (Figures 2 and 3) consists of two stages:

(A) Ultrafast vibrational energy transfer, which is due to repulsion, occurs on the time scale of $\sim$200 fs (Figures 2 and 3). This energy-tansfer process is dominated by the magnitude of the scale parameter $\bar{\sigma}$.

(B) "Slow" energy transfer on the time scale of tens of picoseconds (for $\bar{\sigma} = 1.2$) and up to hundreds of pisoseconds (for $\bar{\sigma} = 1.0$) occurs due to vibrational relaxation of the excimer. The dynamics of the cluster induced by these energy-transfer processes invovles reactive vibrational predissociation, as is apparent from Figures 3 and 4. This state of affairs is, of course, drastically different from that encountered in infinite systems, where a nonreactive process prevails when the phonon modes of the system

are excited. A cursory examination of the dissociative dynamics (Figures 4) of the Ar_{13} cluster following excimer formation indicated that two reactive processes prevail.

(1) A fast stepwise "evaporation" of Ar atoms is exhibited on the time scale of $\sim$10 ps. This process is induced by energy-transfer process A.

(2) Subsequently, an additional reactive process appears (Figure 4), which invovles slower vibrational predissociation of Ar atoms on the time scale $\geq$10 ps. This dissociative process is induced by both energy-transfer processes A and B.

It is imperative to note that the short-time "explosion" of the electronically excited cluster is induced by energy transfer due to short-range repulsive interactions. When these interactions are switched off by taking $\bar{\sigma} = 1.0$, only mechanism B is operative for vibrational energy flow into the cluster and the cluster dissociative process, which again occurs by stepwise "evaporation" occurring on the time scale of 30–1000 ps. The appropriate excited-state repulsive physical parameter characterizing excimer–cluster interactions in RGCs is $\bar{\sigma} = 1.1–1.2$, and we expect the occurrence of energy flow predissociation, induced by excited repulsive interactions, to occur on the time scale $\sim$10 ps.

In order to investigate the dependence of the nature and rate of energy redistribution processes following excitation, on the degree of aggregation, we have performed similar simulations for an Ar_{55} cluster, with the excimer located at either the center or at the outer shell of the cluster. These simulations revealed that while the ultrafast vibrational energy flow from the vibrationally excited excimer to the rest of the cluster is operative (see Figure 5), no fragmentations are observed, i.e., nonreactive vibrational energy redistribution, characteristic to infinite condensed matter systems, prevails. This of course is a direct consequence of the large number of densely spaced available "bath" modes. We note, however, that following the ultrafast energy flow, which occurred on the 0.1–0.3-ps time scale, the subsequent vibrational relaxation
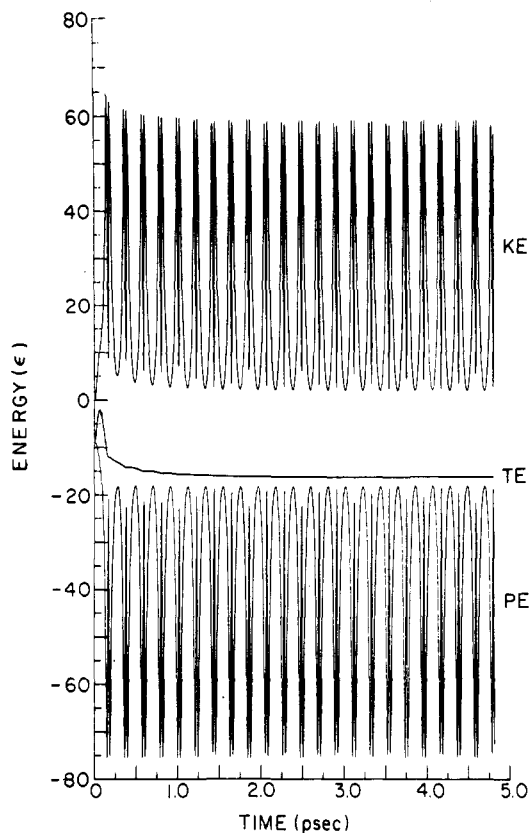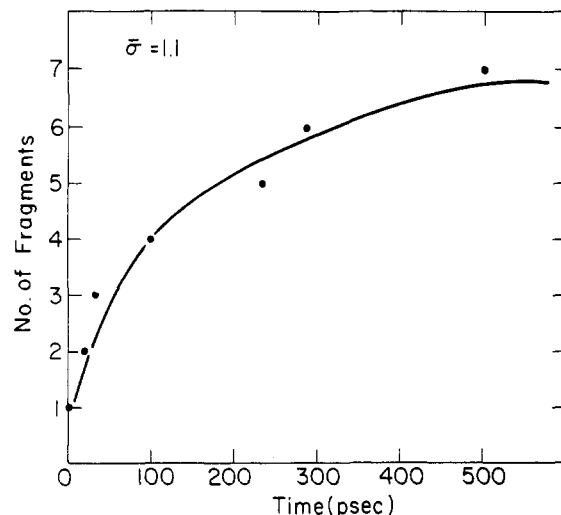
Figure 2. Time dependence of the potential energy (PE), the kinetic energy (KE), and the total energy (TE) of the bare excimer in Ar_{13} ($\bar{\sigma}$ = 1.20). Energies are given in units of ϵ.
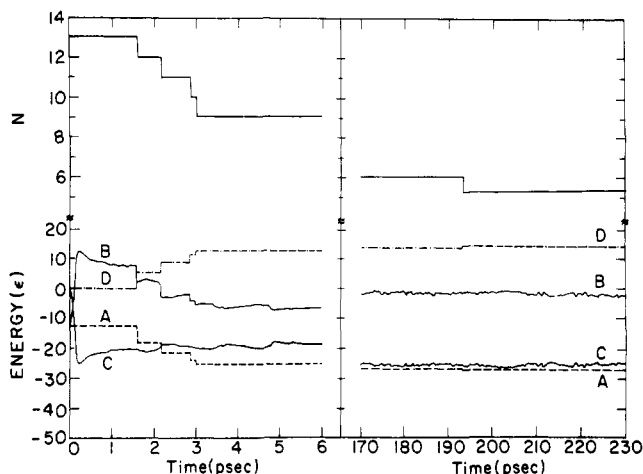

Figure 3. Time evolution of fragmentation dynamics of the electronically excited $(Ar)_{13}$ cluster ($\bar{\sigma}$ = 1.15). (A) Total energy of the main fragment. (B) Total energy of the "bath subsystem". (C) Total energy of the "reaction center". (D) Kinetic energy of the dissociated atoms. (E) Number of atoms in the main fragment. The steps in curves A, D, and E mark the stepwise dissociation of individual Ar atoms from the main fragment.

rate is rather slow, due to the frequency mismatch and local dilation effects.

We conclude this section with a few observations on mixed clusters. We have performed extensive studies of $Ar_{n-m}Xe_m{}^*$ cluster, with n = 13, 55 and m = 1, 2, with the Xe atoms located at either the center or on the outer shell. In the case of $Ar_{12}Xe^*$, with the Xe^* centrally located, the excited atom escaped from the cluster on a time scale of 50 ± 20 ps. In view of the fast escape, we predict that the radiative decay will be characteristic of the free excited atom rather than from the cluster-shifted species. Curiously, we observed no such phenomenon for $Ar_{54}Xe^*$ or $Ar_{53}Xe_2{}^*$ (either centrally or peripherally locating the excitations). In these systems the effectiveness of the cluster-mediated vibra-

Figure 4. The time evolution of the fragmentation of the electronically excited Ar_{13} cluster ($\bar{\sigma}$ = 1.10). Note the sequential "evaporation" of the single ground-state Ar atoms.
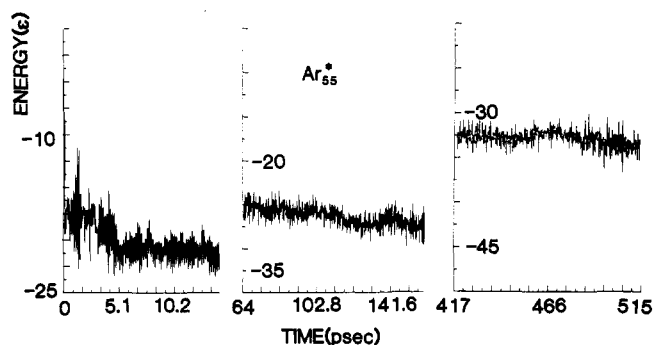
Figure 5. Time dependence of the total internal energy of the bare excimer in Ar_{55} ($\bar{\sigma}$ = 1.1).

tional relaxation dominates, aided by characteristics of the interaction potentials and the heavy mass of the impurity (the defect modes are embedded within the vibrational manifold of the host cluster).

3. Electron Localization and Cluster Isomerization Induced by Electron Attachment

The physical and chemical phenomena associated with the attachment of an excess electron to a molecular cluster are of considerable interest because of two reasons. First, quantum phenomena are expected to be pronounced in such finite systems, where the electron wavelength is comparable to the cluster size. Second, the excess electron can serve as a probe for the nuclear motion and dynamics of the cluster.

Electron attachment may occur via reactive or nonreactive channels where, in the latter, electron attachment is not accompanied by the breaking of either intermolecular or intramolecular bonds and can result in either bulk or surface states of the excess electron. From the point of view of general methodology, the formation of electron surface states on clusters is facilitated by the large surface-to-volume ratio of clusters. From the technical point of view, the formation of such surface states is dominated by the structure of the cluster and by the nature of the electron–cluster interaction. Internal localization of the electron on the other hand tends to occur in moderately large clusters which contain an anion vacancy. We demonstrate these modes of localization through investigations of electron attachment to $[Na_{14}Cl_{13}]^+$ and $[Na_{14}Cl_{12}]^{2+}$.

When a nonreactive attachment of an excess electron to a cluster results in a localized state, which has no parentage in the atomic (or molecular) states of the individual cluster constituents, the cluster nuclear structure may undergo substantial reorganization.[5] Investigations of the energetics of cluster isomerization induced by electron attachment are facilitated by our studies of e^- +

$(NaCl)_4$ over a wide range of temperatures.[18] The alkali-halide clusters (AHCs) were chosen for three reasons. First, the nature of interionic interactions in these clusters is well understood.[19,20] Second, there exists an abundance of model calculations on both neutral and charged ACHs.[19] Third, quite extensive information is available on electron–alkali cation[21,22] (M^+) and electron–halide anion (X^-) interactions.

3.1. The Quantum Path Integral Molecular Dynamics Method (QUPID).[5,22–25]

The structure and energetics of an e–AHC system has been explored by the quantum path-integral molecular dynamics (QUPID) method. This approach, which rests on a discrete version of Feynman's path integral method, provides a powerful method for the study of these systems. In this scheme the quantum problem is isomorphic to an appropriate classical problem, with the excess electron being mapped onto a closed flexible polymer of P points. The isomorphism becomes exact as $P \rightarrow \infty$. The practical applicability of the computational method rests on the development of numerical algorithms, which achieve convergence with manageable values of P.

The Feynman path integral formulation of quantum statistical mechanics[26] allows a derivation of an approximate expression for the partition function, Z, for a system consisting of a quantum particle (mass m and coordinate $\vec{r}$), interacting with a set of N classical particles (whose phase space trajectories are generated by classical equations of motion) via a potential $V(\vec{r},\vec{R}_1,...,\vec{R}_N)$

$$Z = \left(\frac{mP}{2\pi\hbar^2\beta}\right)^{3P/2} \int d\vec{r}_1...d\vec{r}_p \, d\vec{R}_1...d\vec{R}_N e^{-\beta V_{eff}} \quad (1a)$$

where

$$V_{eff} \equiv \sum_{i=1}^{P} \frac{mP}{2\hbar^2\beta^2}(\vec{r}_i - \vec{r}_{i+1})^2 + \frac{1}{P}\sum_{j=1}^{N}\sum_{i=1}^{P}V(\vec{r}_i,\vec{R}_j) + V_c(\vec{R}_1,...,\vec{R}_N) \quad (1b)$$

V_c is the interaction potential between the classical particles, and $\beta = (k_B T)^{-1}$.

Equations 1a and 1b establish an isomorphism[23] between the quantum problem and a classical one in which the quantum particle is represented by a flexible periodic chain (necklace) of P pseudoparticles (beads) with nearest-neighbor harmonic interactions with a temperature-dependent spring constant, $Pm/\hbar^2\beta^2$. The above expression for the partition function is exact as $P \rightarrow \infty$. In practice, the finite value of P employed in a calculation is chosen to yield convergent results and depends upon the temperature and characteristics of the interaction potential, V.

The average energy of the system at equilibrium is given by

$$E = \frac{3N}{2\beta} + \langle V_c \rangle + K + \frac{1}{P}\langle\sum_{i}^{P}V(\vec{r}_i)\rangle \quad (2a)$$

where

$$K = \frac{3}{2\beta} + \frac{1}{2P}\sum_{i=1}^{P}\left\langle \frac{\partial V(\vec{r}_i)}{\partial\vec{r}_i} \cdot (\vec{r}_i - \vec{r}_P) \right\rangle \quad (2b)$$

and the angular brackets indicate statistical averages over the probability distribution as defined in eq 1. The first two terms in Eq 2a are the mean kinetic and potential energies of the classical component of the system. The quantum particle kinetic energy estimator,[27] K, consists of the free particle term ($K_f = 3/2\beta$) and

a contribution due to the interaction (K_{int}). Finally, the last term in eq 2a is the mean potential energy of interaction between the quantum particle and the classical field.

A measure of the quantum character of the system may be inferred from the relative contribution of K_{int} to the kinetic energy K. The magnitude of K_{int} depends on two factors, the gradients of the potential at the location of the beads and the bead spatial distribution. For a classical particle whose thermal wavelength, $\lambda_T = (\beta\hbar^2/m)^{1/2}$, approaches zero, the Gaussian factor in eq 1a (see first term in eq 1b) reduces to a δ function ($\delta(\vec{r}_i - \vec{r}_{i+1})$, for all i) and the necklace collapses to a single point, representing a classical particle. Under this circumstance $K_{int} = 0$. Generally, the degree of quantal character depends upon the interplay between the spatial extent of the particle (which in the above formulation is related to the spatial distribution of the pseudo-particles) and a characteristic length associated with the rate of change of the potential.

Another convenient measure of the quantum character of the system and the degree of localization of the quantum particle is provided by the complex time correlation function[28]

$$R^2(t - t') = \langle |\vec{r}(t) - \vec{r}(t')|^2 \rangle \quad (3)$$

where $|\vec{r}(t) - \vec{r}(t')|$ is the distance between two points (beads) on the electron path separated by a "time" $(t - t') \in (0,\beta\hbar)$. The value at $t - t' = \beta\hbar/2$, $R \equiv R(\beta\hbar/2)$, characterizes the breadth of the bead distribution and yields the correlation length. Note that for a free particle, where the bead distribution obeys Gaussian statistics, $R_f = 3^{1/2}\lambda_T/2$. For a localized state, when fluctuations in $R(t - t')$ are inhibited, $R(t - t')$ is dominated by the ground state,[28] and as a function of $(t - t')$, $R^2(t - t')$ starts from zero at $t - t' = 0$ and rapidly achieves a constant value, with $R < R_f$ (i.e., it is independent of "time" except for $t - t'$ close to 0 and $\beta\hbar$). The rise time, τ, is a (rough) measure of the excitation energy $\Delta E \equiv E_1 - E_0$ (where E_1 is a Boltzmann weighted average of the manifold of excited states), given by $\Delta E = \hbar/\tau$. A delocalized state, on the other hand, is characterized by a dependence of $R^2(t - t')$ on $(t - t')$ over the whole range $(0,\beta\hbar)$.

The formalism described above is converted into a numerical algorithm by noting the equivalence[22] between the equilibrium statistical averages over the probability distribution given in eq 1 and sampling over phase space trajectories, generated by a classical Hamiltonian

$$H = \sum_{i=1}^{P}\frac{m^*\dot{\vec{r}}_i^2}{2} + \sum_{i=1}^{N}\frac{M_I\dot{\vec{R}}_I^2}{2} + \sum_{i=1}^{P}\left[\frac{Pm}{2\hbar^2\beta^2}(\vec{r}_i - \vec{r}_{i+1})^2 + \frac{V(\vec{r}_i)}{P}\right] + V_c(\vec{R}_1,...,\vec{R}_N) \quad (4)$$

where m^* is an arbitrary mass chosen such that the internal frequency of the necklace, $\omega = [mP/(m^*\beta^2\hbar^2)]^{1/2}$, will match the other frequencies in the system, and M_I is the mass of a classical particle. For a description of the application of the method to a wide variety of quantum many-body systems of chemical and physical interest the reader is referred to a recent review.[29]

3.2. Electron Localization in Charged Clusters.

To investigate the modes of electron localization in clusters we have performed QUPID simulations of electron interaction with $[Na_{14}Cl_{13}]^+$ and $[Na_{14}Cl_{12}]^{2+}$, at 300 K. The structure of the bare clusters is cubic[19] (with small distortions) and the doubly charged one contains an internal anion vacancy. The ions were treated as classical particles interacting via Coulomb interaction and Born–Mayer repulsion.[19,20]

The interaction of the electron consists of a sum of electron–ion potentials: pure Coulomb repulsion for the e–anion interaction[22] and a pseudo-potential $-e^2/R_c$ for $r \leq R_c$ and $-e^2/r$ for $r > R_c$ for the e–cation[21,22] (for Na^+, $R_c = 3.24a_0$). On the basis of the examination of the stability of the variance of the kinetic energy

(18) Scharf, D.; Landman, U.; Jortner, J., *J. Chem. Phys.*, in press.
(19) Martin, T. P. *Phys. Rep.* **1983**, *95*, 167.
(20) Fumi, F. G.; Tosi, M. P. *J. Phys. Chem. Solids* **1964**, *25*, 31, 45.
(21) Shaw, R. W. *Phys. Rev.* **1968**, *174*, 769. See also QUPID Studies of e + Na$^+$ and (NaCl)$^-$ in Scharf, D.; Jortner, J.; Landman, U. *Chem. Phys. Lett.*, **1986**, *130*, 504.
(22) Parrinello, M.; Rahman, A. *J. Chem. Phys.* **1984**, *80*, 860.
(23) Chandler, D.; Wolynes, P. G. *J. Chem. Phys.* **1981**, *79*, 4078.
(24) De Raedt, B.; Sprik, H.; Klein, H. L. *J. Chem. Phys.* **1984**, *80*, 5719.
(25) Chandler, D. *J. Phys. Chem.* **1984**, *88*, 3400.
(26) Feynman, R. P.; Hibbs, A. R. *Quantum Mechanics and Path Integrals*; McGraw-Hill: New York, 1965.

(27) Herman, M. F.; Bruskin, E. J.; Berne, B. J. *J. Chem. Phys.* **1982**, *76*, 5150.
(28) Nichols, A. L.; Chandler, D.; Singh, Y.; Richardson, D. M. *J. Chem. Phys.* **1984**, *81*, 5109.
(29) Berne, B. J.; Thirumalai, D. *Annu. Rev. Phys. Chem.* in press.
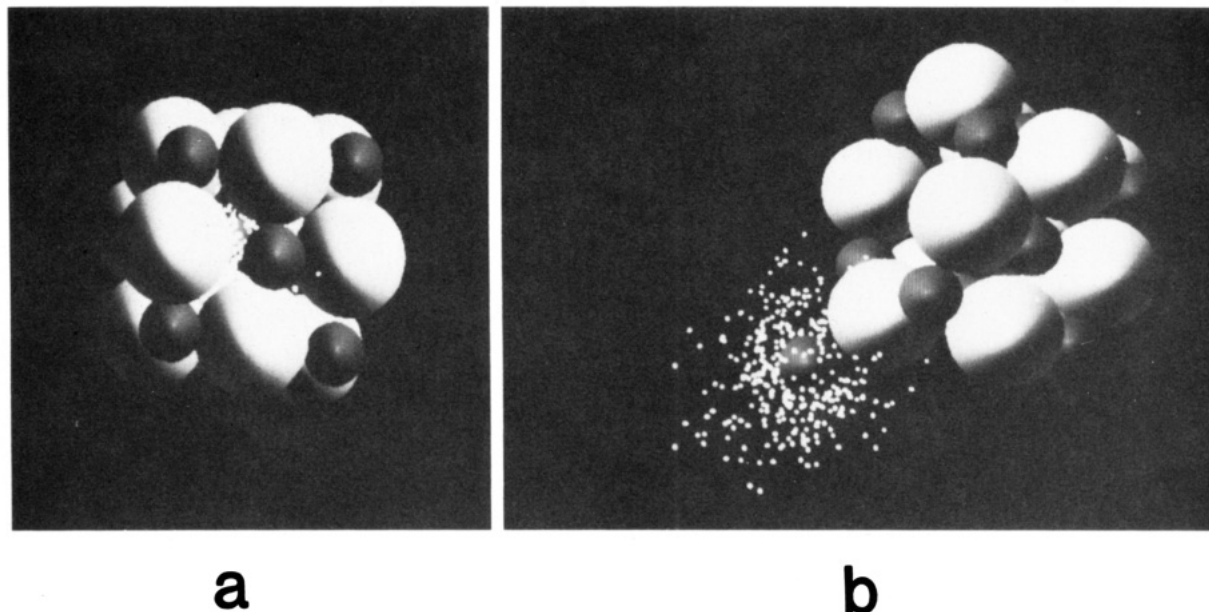
Figure 6. Cluster configurations for (a) e–$[Na_{14}Cl_{12}]^{2+}$ and (b) e–$[Na_{14}Cl_{13}]^{+}$, exhibiting internal and external electron localization, respectively. Large and small balls, Cl^- and Na^+, respectively. Small dots represent the electron distribution.

TABLE I: Energetics of Electron Attachment to Charged Clusters (in hartrees)

	$[Na_{14}Cl_{13}]^{+}$	$[Na_{14}Cl_{12}]^{+}$
E_B^e	−0.1594	−0.2490
E_c	0.1055	0.0799
E_A	−0.0539	−0.1691

contribution K_{int}, the number of "electron beads" was taken as $P = 399$. An integration step of $\Delta t = 1.03 \times 10^{15}$ s was employed, and long equilibration runs were performed ($(1-2) \times 10^4 \Delta t$). The reported results were obtained via averaging over $8 \times 10^3 \Delta t$ following equilibration.

In Figure 6, a and b, we present our results for the equilibrium electron charge distribution (small dots) and for the nuclear configuration of the clusters. The energetics of these systems may be summarized in terms of the electron affinity, E_A, of the cluster

$$E_A = E_B^e + E_c \tag{5}$$

which is obtained by summing the electron binding energy

$$E_B^e = 3/2\beta + K_{int} + P^{-1}\sum_{i=1}^{P} \langle V_e(\vec{r}_i) \rangle \tag{6}$$

and the cluster reorganization energy

$$E_c = \langle V_{AHC} \rangle - \langle V_{AHC} \rangle_0 \tag{7}$$

where $\langle V_{AHC} \rangle_0$ is the potential energy of the "bare" AHC in the absence of the electron. Our results concerning the energetics of electron attachment are given in Table I.

As is apparent from Figure 6a the $[Na_{14}Cl_{12}]^{2+}$ cluster stabilizes an internally localized electron state, with the ionic configuration similar to that found in a bulk F^- center defect, thus establishing the dominance of short-range interactions for internal electron localization.

A drastically different localization mode is obtained in the $[Na_{14}Cl_{13}]^{+}$ system (Figure 6b), where a novel surface state is exhibited. We refer to this state as a cluster surface localized state.[5] Such surface states were considered for macroscopic alkali halide crystals by Tamm about 50 years ago but were never experimentally documented. Finally, it is of interest to note that the total energy of e–$[Na_{14}Cl_{12}]^{2+}$ is close to that of the $[Na_{14}Cl_{13}]^{+}$, whereupon the electron (internal) binding energy in the cluster is similar to that of a negative ion.

3.3. Cluster Isomerization Induced by Electron Attachment. While for charged clusters of intermediate size electron localization is not accompanied by major structural rearrangement (see section

3.2), such effects may be found for smaller systems.[5] Moreover, we found[18] that electron attachment may induce configurational transformations in small neutral ionic clusters at relatively low temperatures, and that the equilibrium configurations of the cluster with the attached electron do not necessarily relate to those of the parent neutral cluster.

Our QUPID simulations of electron interaction with Na_4Cl_4 clusters at various temperatures employed the same interaction potentials described in section 3.2. In these studies we have used constant-temperature simulations,[30] with a velocity form of the Verlet algorithm. The numbers of "electron beads", P, were taken as 1000, 520, 520, and 250 for $T = 50$, 575, 750, and 1000 K, respectively. Prolonged runs were performed to assure proper sampling of the accessible phase space and thus numerically reliable averaged quantities.

Equilibrium configurations at various temperatures are shown in Figure 7. At low T ($T \leq 500$ K) the electron distribution is extended with an equal probability charge distribution around all the four Na^+ ions, and the ionic configuration is similar to that of the low-T neutral cluster. It is likely that, in the low-temperature domain, symmetry considerations dominate and determine the mode of localizations. At the intermediate temperture domain, 500 K $\leq T \leq$ 750 K, a configurational change of the negative cluster is exhibited (see Figure 7b). This is a distorted planar configuration and is similar to the stable structure of the related classical $Na_4Cl_5^-$ cluster, which we found in simulations performed in the range 50 K $< T <$ 1300 K. At the high-T domain, 750 K $< T <$ 1200 K, a coexistence of several isomers is found. At ~750 K a boatlike configuration (Figure 7c) dominates (in this range a bent chain is also found) and at $T \sim 1000$ K an elongated chain in coexistence with a planar ring (Figure 7, d and e) is found. We observe a tendency toward spatial localization of the electron upon increase in T. Furthermore, the presence of the excess electron induces two types of configurational modifications which are either quantitatively or qualitatively different from those in the neutral cluster:

(1) The localized excess electron can play the role of a pseudonegative ion, with appreciable kinetic energy, which is overwhelmed by the electron potential energy, leading to new nuclear configurations which have no counterpart in the neutral cluster.

(2) The partial neutralization of a single positively charged ion by the excess electron results in the appearance of the high-T configuration of the neutral parent cluster at substantially lower temperatures for the negatively charged cluster. The first effect

(30) Fox, J. R.; Anderson, H. C. *J. Phys. Chem.* **1984**, *88*, 4019.
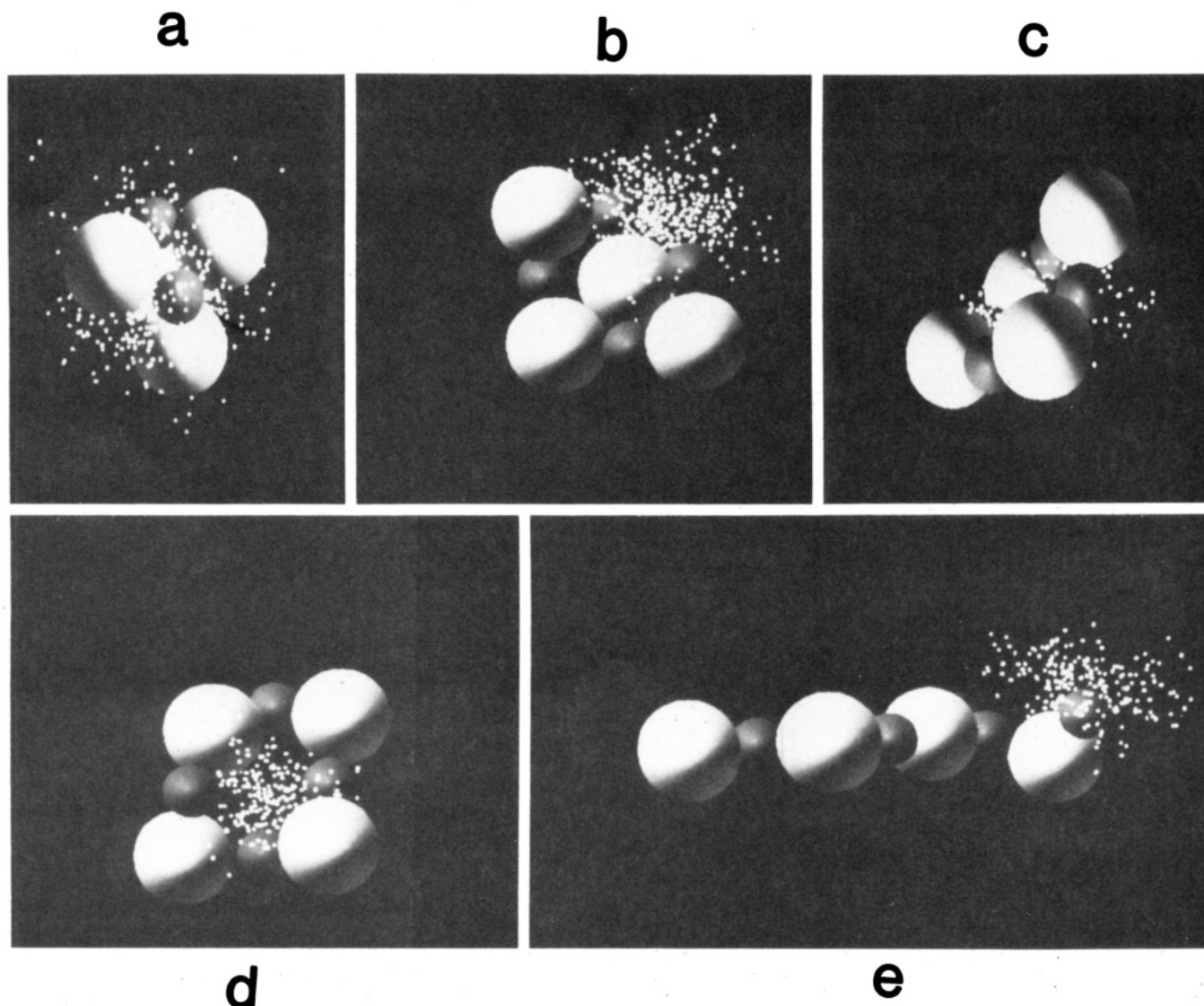
Figure 7. Cluster configurations for e–Na_4Cl_4: (a) 50 K, (b) 575 K, (c) 750 K, (d, e) 1000 K. See caption to Figure 6.

is observed in the intermediate T range, while both effects are exhibited in the high-T domain.

The electron affinity, E_A, of the $[Na_4Cl_4]$ cluster at low T is calculted to be 0.029 ± (8×10^{-3}) hartrees, which is considerably lower than the EA of the intermediate size positive ionic clusters. Further energetics and other characteristics of the clusters are given in Table II.

4. Electron Attachment to Water Clusters

A solvated electron is a bound excess electron state in a polar fluid. The nature of the electron states in such media may be either spatially extended (diffuse electron distribution) or highly compact. In either case binding of the electron may be accompanied by large solvent reorganization. A water molecule, which has a closed-shell electronic configuration, isoelectronic to Ne, does not bind an electron (as long as unusually distorted nuclear configurations are excluded). On the other hand, electrons can be trapped in liquid or solid water and in high density vapor.[7,32–34] The nature of the solvated electron and the formation mechanism of $(H_2O)_n^-$ have been the subject of various theoretical treatments

TABLE II: Total Energies of the Neutral and Negatively Charged Clusters[a]

	50 K	575 K	750 K	1000 K
$E(Na_4Cl_4)$	−1.0244	−1.0010	−1.0049	−0.9978
$E(Na_4Cl_4^-)$	−1.053	−1.00	−0.99	−0.96
	(8×10^{-3})	(2×10^{-2})	(2×10^{-2})	(3×10^{-2})
λ_T	68	23	20	17
$R(\beta\hbar/2)/R_f$	0.09	0.33	0.39	0.42
Q	99%	95%	93%	90%

[a] The calculated thermal wavelength, λ_T, localization parameter, $R(\beta\hbar/2)/R_f$, and degree of quantum character, $-Q = (K - K_f)/K$ (eq 2b), are given. Energy and length in atomic units. Variances in parentheses.

from continuum dielectric models to quantum-mechanical calculations.[4,35] While these studies have advanced our knowledge, the recent addition of quantum simulations (see section 3) to our theoretical arsenal opens new avenues in studies of bulk[36,37] and cluster[5,38] solvation.

A key issue in modeling the system is the choice of interaction potentials. Fortunately, for small water clusters, interaction

(31) Landman, U.; Barnett, R. N.; Cleveland, C. L.; Norlander, P. In *Tunneling*, Jortner, J., Pullman, B., Eds.; Reidel, New York; 1986.

(32) *J. Phys. Chem.* **1984**, *88*, 3699–3914. *Electrons in Fluids*, Jortner, J., Kestner, P. N., Eds.; Springer: New York, 1973.

(33) Haberland, H.; Schindler, H. G.; Worsnop, D. R. *Ber. Bunsen-Ges. Phys. Chem.* **1984**, *88*, 270. *J. Phys. Chem.* **1984**, *88*, 3903. *J. Chem. Phys.* **1984**, *81*, 3742. Preprint on field detachment of $(H_2O)_2^-$.
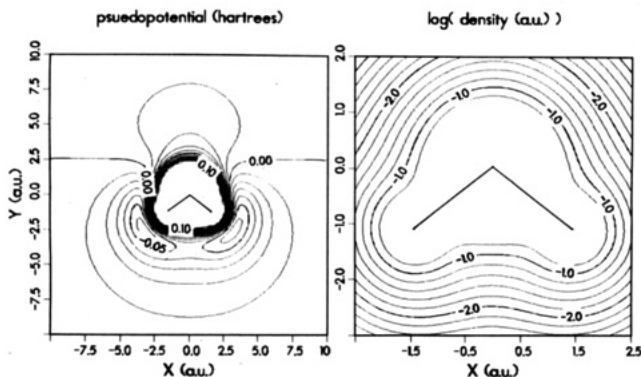
(34) Coe, J. V.; Worsnop, D. R.; Bowen, K. H. *J. Chem. Phys.*, in press.

(35) Rao, B. K.; Kestner, N. R. *J. Chem. Phys.* **1984**, *80*, 1587, and references therein.

(36) Sprik, M.; Impey, R. W.; Klein, M. L. *J. Chem. Phys.* **1985**, *83*, 5802.

(37) Jonah, C. D.; Romero, C.; Rahman, A. *Chem. Phys. Lett.* **1986**, *123*, 209.

(38) Wallquist, A.; Thirumalai, D.; Berne, B. J. *J. Chem. Phys.* **1986**, *85*, 1583.

pseudopotential (hartrees)   log(density (a.u.))

Figure 8. Contours of electron–water interaction, left, and of the electronic density (log $\rho(r)$), right, see eq 8, in the plane containing the nuclei. The oxygen is located at the origin.

potential functions which provide a satisfactory description for a range of properties are available.[39,40] We have used the RWK2-M model[40] for the intra- and inter-water interactions. Less is known about the electron–water interaction.[37,38]

We have constructed a pseudopotential which consists of Coulomb, polarization, exclusion, and exchange contributions:

$$V(\vec{r}_e,\vec{R}_o,\vec{R}_1,\vec{R}_2) = V_{coul} + V_{pol} + V_{excl} + V_x \quad (8a)$$

The positions of the oxygen and hydrogen nuclei of the water molecule are given by $(\vec{R}_o,\vec{R}_1,\vec{R}_2)$ and $\vec{r}_e$ is the position of the electron.

The Coulomb interaction is

$$V_{coul}(\vec{r}_e,\vec{R}_o,\vec{R}_1,\vec{R}_2) = -\sum_{j=1}^{3} q_j e/\max(|\vec{r}_e - \vec{R}_j|,R_{cc}) \quad (8b)$$

where $\vec{R}_3 = \vec{R}_o + (\vec{R}_1 + \vec{R}_2 - 2\vec{R}_o)\delta$ is the position of the negative point charge of the RWK2-M model; $q_1 = q_2 = 0.6e$, $q_3 = -1.2 e$, and $\delta = 0.22183756$. The value of q_j and δ were chosen[39,40] to give a good representation of the dipole and quadrupole moments of the water monomer. The cutoff radius, R_{cc}, was taken to be $0.5a_0$, and the results are insensitive to the precise value of R_{cc}.

The polarization interaction is given by

$$V_{pol}(\vec{r},\vec{R}_o) = -0.5\alpha e^2/(|\vec{r}_e - \vec{R}_o|^2 + R_p^2)^2 \quad (8c)$$

where $\alpha = 9.7446$ au is the spherical polarizability of the water molecule. The form of V_{pol} and the value of $R_P = 1.6a_0$ were chosen to fit approximately the adiabatic polarization potential as calculated by Douglass et al.[43] for an approach of the electrons along the H–O–H bisector (see Table 7 and Figure 2 in ref 43).

The exclusion, V_{excl}, and exchange, V_x, contributions both require the electron density, $\rho(\vec{r},\vec{R}_o,\vec{R}_1,\vec{R}_2)$, of the water molecule. We find that a reasonable fit to the calculated electron density,[42] in the regions of importance, is provided by

$$\rho(\vec{r};\vec{R}_o,\vec{R}_1,\vec{R}_2) = 8a_0^{-3}e^{-3|\vec{r}-\vec{R}_o|/a_0} + a_0^{-3}\sum_{j=1}^{2}e^{-3|\vec{r}-\vec{R}_j|/a_0} \quad (8d)$$

A contour plot of log ρ for $\vec{r}$ in the plane of the molecule is shown on the right of Figure 8.

(39) Reimers, J. R.; Watts, R. O.; Klein, M. L. *Chem. Phys.* **1982**, *64*, 95.

(40) Reimers, J. R.; Watts, R. D. *Chem. Phys.* **1984**, *85*, 83. This paper as well as the description of the potential in ref 39 (eq 13 and Table 1) contain several ambiguities and typographical errors. When corrected we reproduce their results.

(41) Bardsley, J. N. *Case Stud. At. Phys.* **1974**, *4*, 299. Kleiman, G. G.; Landman, U. *Phys. Rev. B* **1973**, *8*, 5484.

(42) Kerr, C. W.; Karplus, M. In *Water, A Comprehensive Treatise*, Franks, F., Ed.; Plenum: New York, 1972; p 21. Ribarsky, M. W.; Luedtke, W. D.; Landman, U. *Phys. Rev. B* **1985**, *32*, 1430.

(43) Douglass, Jr., C. H.; Weil, D. A.; Charlier, P. A.; Eades, R. A.; Truhlar, D. G.; Dixon, D. A. *Chemical Applications of Atomic and Molecular Electrostatic Potentials*, Politzer, P., Truhlar, D. G., Ed.; Plenum: New York, 1981; p 173.
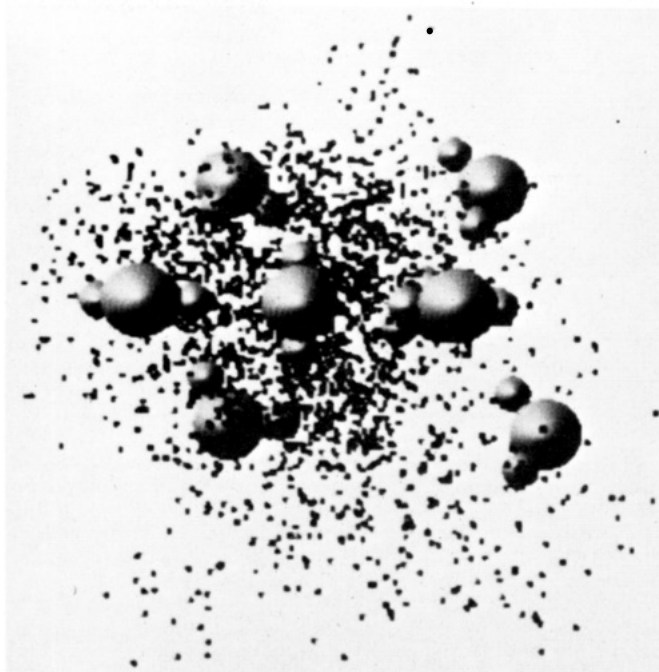
Figure 9. The equilibrium electron distribution (small dots) in $(H_2O)_8^-$ for the molecular configuration given in ref 35.

The repulsion, due to the exclusion principle, is modeled as a "local kinetic energy" term[41]

$$V_{excl}(\vec{r}_e,\vec{R}_o,\vec{R}_1,\vec{R}_2) = 0.5e^2a_0(3\pi^2\rho)^{2/3} \quad (8e)$$

The exchange interaction is modeled via the local exchange approximation[44]

$$V_x(\vec{r}_e,\vec{R}_o,\vec{R}_1,\vec{R}_2) = -\alpha_x e^2a_0(3\pi^2\rho)^{1/3}/\pi \quad (8f)$$

The parameter α_x was taken to be $\alpha_x = 0.3$ in order to obtain good agreement between our simulation results and the SCF results[35] for a given arrangement of molecules (see below).

A contour plot of the total electron–water pseudopotential, eq 8a, is shown on the left of Figure 8 (in the plane of the molecule, with the oxygen located at the origin).

In our quantum-path-integral molecular dynamics simulations (section 3) the water molecules are treated classically (there is no evidence of an isotope effect on solvation) while the quantum electron "necklace" contains a number of beads (P) which depends on the temperature (T). We have found that, as a rule of thumb, adequate discretization is obtained if $Pk_BT \geq e^2/a_0$. In order to test our newly proposed electron–water pseudopotential and to evaluate the parameter α_x (eq 8f), we performed calculations for an $(H_2O)_8^-$ cluster with the molecules held fixed (static) in the "tetrahedral cage" geometry used in the SCF calculations of Rao and Kestner.[35] We determined that $\alpha_x = 0.3$ gave good agreement with the "scaled" SCF results for the vertical binding energy (–0.026 hartrees as compared to the SCF results of –0.024 hartrees). The results for $(H_2O)_8^-$ are summarized in the first column of Table III. All of the results in the table are from MD runs to typically 5×10^4 steps following equilibration. A shorter run at $k_BT = 0.0050$ hartrees ($P = 2048$) for the $(H_2O)_8^-$ static cluster gave the same results for the vertical binding energy. We point out that the tetrahedral cage geometry was designed to maximize the binding of the electron[35] and is in fact highly unstable. The cluster reorganization energy (E_c) is large, and if the molecules are allowed to move the structure falls apart immediately.

We turn now to an investigation of electron attachment to a water dimer, which has been the subject of recent experimental[33] and theoretical[38,45] studies. We have performed a simulation at

(44) See e.g., Truhlar, D. G. In *Chemical Applications of Atomic and Molecular Electrostatic Potentials*, Politzer, P., Truhlar, D. G., Eds.; Plenum: New York, 1981; p 123.

(45) Chipman, D. *J. Phys. Chem.* **1978**, *82*, 1980.

TABLE III: Energetics of $(H_2O)_n^-$ Clusters, $n = 2$, 8, and 18[a]

| cluster	$(H_2O)_8^-$ "static cage"	$(H_2O)_2^-$	$(H_2O)_{18}^-$ "internal"	$(H_2O)_{18}^-$ "surface"
$k_B T$	0.00025	0.0000625	0.00025	0.00025
no. of beads	4096	16384	4096	4096
PE(inter)	−0.0174	−0.0100 (0.0003)	−0.2195 (0.0054)	−0.2523 (0.0039)
PE[neutral]	−0.1126 (0.0026)	−0.0100 (0.0003)	−0.3027 (0.0038)	−0.3027 (0.0038)
PE(intra)	0.0045	0.0006 (0.0003)	0.0249 (0.0036)	0.0258 (0.0035)
PE[neutral]	0.0103 (0.0023)	0.0006 (0.0003)	0.0272 (0.0037)	0.0272 (0.0037)
E_c	0.0894	0.0000	0.0809	0.0490
PE(e−water)	−0.0727 (0.0025)	−0.0008 (0.0001)	−0.1543 (0.0062)	−0.0920 (0.0023)
KE_{int}	0.0489 (0.0054)	0.0007 (0.0014)	0.0823 (0.0071)	0.0438 (0.0043)
EBE(vertical)	−0.0238 (0.0059)	−0.0001 (0.0014)	−0.0720 (0.0088)	−0.0482 (0.0046)
EBE(adiabatic)	0.0656	−0.0001	0.0089	0.0008
R_g	6.2	36.0	4.1	5.5
R_T	108	220	108	108
$R(\beta\hbar/2)/R_f$	0.16	0.49	0.11	0.14

[a] The rows labeled [neutral] are the equilibrium quantities for a neutral cluster + free electron. The quantities in parentheses are standard deviations. The molecular configuration for $(H_2O)_8^-$ was fixed as given in ref 35 (the [neutral] results are for an equilibrated cluster, i.e., not the structure of ref 35). E_c is the molecular reorganization energy. EBE is the electron binding energy: EBE (vertical) = PE(e−water) + KE_{int}, EBE (adiabatic) = EBE (vertical) + E_c. Energies are in hartrees and lengths in bohr radii (a_0).
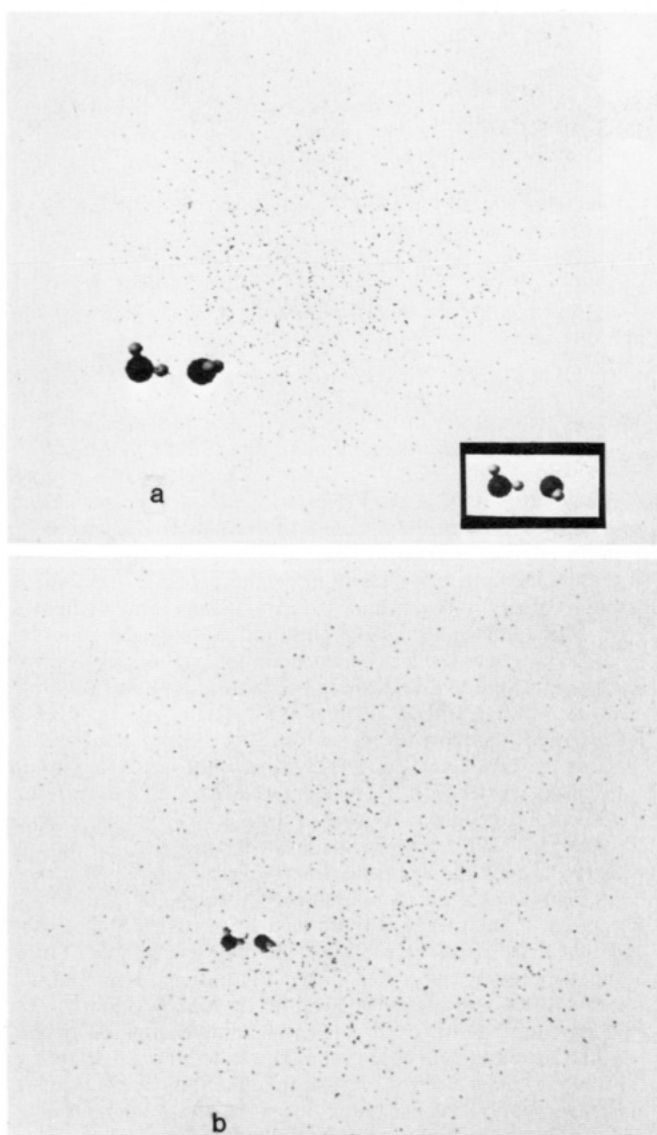
Figure 10. (a) The high-dipole configuration contributing to the metastable state of $(H_2O)_2^-$ at $T = 20$ K. In the inset the configuration of a neutral water dimer is shown. (b) The equilibrium configuration of $(H_2O)_2^-$. Note the diffuseness of the electron distribution.

$T = 20$K ($k_B T = 0.0000625$ hartrees), with $P = 16384$ beads and the results are summarized in the second column of Table III. The simulation started by first equilibrating the system with P
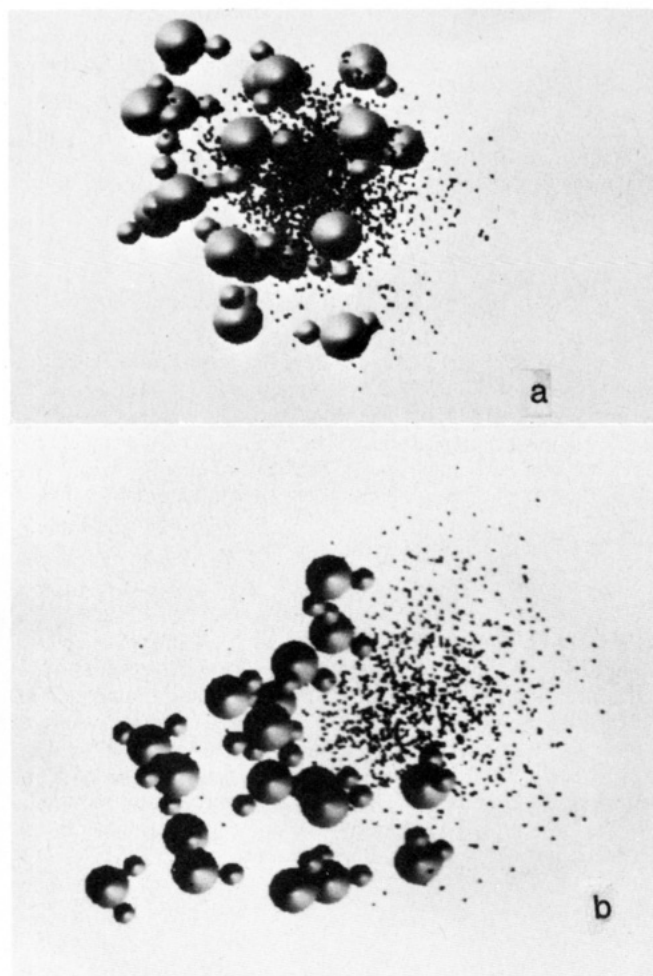
Figure 11. Molecular and electron configurations in the $(H_2O)_{18}^-$ "internal" and "surface" states, (a) and (b), respectively.

= 1024, then doubling the number of beads and reequilibrating four times. While the uncertainty in the results is large, it does appear that the electron is bound in a diffuse state, with a binding energy of about 3 meV, and that the molecular configuration is essentially that of a neutral dimer.

During the initial equilibration runs the system of the water dimer and necklace spent a long "time" in an apparent metastable state in which the bead distribution was more compact (R_g = 15–30 au) and during which the dimer configuration fluctuated between that of the neutral dimer (insert in Figure 10) and the configuration shown in Figure 10a; the dipole moment during this

period fluctuated between 1.2 and 1.7 au, and the vertical binding energy obtained from this time period is about $(5-10) \times 10^{-4}$ hartree. It is interesting to note that the results obtained from this "metastable state" are consistent with an estimate of the binding energy (17 meV) obtained from field detachment.[33]

The vertical ionization energies of $(H_2O)_n^-$ for $n > 10$ have been recently measured by photoelectron spectroscopy.[34] The values found are $-0.7 \geq$ EBE (vertical) ≥ -1.2 eV for $11 \leq n \leq 20$. Motivated by these results and by previous predictions[46] about the stability and geometry of $(H_2O)_n^-$ we have embarked upon systematic studies of electron attachment to clusters in this size range. Our results at this stage of the investigation, for $(H_2O)_{18}^-$, are given in the last two columns of Table III and the cluster configurations are shown in Figure 11.

The "internal" configuration, shown in Figure 11a, was obtained by first condensing the water molecule around a classical negatively charged particle with a radius of $5a_0$, and subsequently replacing the classical particle with the electron necklace. The vertical EBE of this internally localized state is nearly twice the experimental value; the cluster reorganization energy is large and in fact the adiabatic EBE (the difference between the energies of $(H_2O)_n^-$ and $(H_2O)_n + e^-$) is large and positive, indicating that the state is unstable with respect to the equilibrium neutral cluster and free electron.

The "surface" state (last column of Table III and Figure 11b) was obtained by initially placing a compact distribution of beads next to an equilibrated neutral cluster. The vertical EBE of this state is -1.31 eV, in agreement with the photoelectron spectroscopy results. The adiabatic EBE, while still positive, is very small.

On the basis of these results we conclude that, in the experimentally observed $(H_2O)_n^-$ clusters in this size range, the excess electron probably occupies a surface state rather than an internally localized state and that such negatively charged clusters may in fact be stable with respect to the neutral cluster plus free electron state. It is interesting to note that in recent experiments[47] long-lived water cluster ions were formed by electron attachment to preformed, cold water clusters unlike the previous[33,34] method of preparation where the electrons were injected into the condensation zone of a supersonic jet of water vapor. In these new experiments the electron attachment occurred resonantly at energies very close to zero. The authors suggested that the mechanism for initial localization of the electron could be provided by a surface state.

Our calculations have employed realistic potentials, i.e., inter- and intramolecular interaction potentials as well as a newly developed electron–H_2O pseudopotential which incorporates the essential physics of the interaction and goes beyond oversimplified descriptions such as point–dipole or mere Coulomb interactions. We have demonstrated that quantum simulations provide significant insight into the energetics and mechanisms of electron solvation in clusters. In further studies the dependence on cluster size and temperature and possible improvements of the pseudopotential will be explored.

Registry No. NaCl, 7647-14-5; H_2O, 7732-18-5.

(46) Kestner, N. R.; Jortner, J. *J. Phys. Chem.* **1984**, *88*, 3818.

(47) Knapp, M.; Echt, O.; Kreisle, D.; Recknagel, E. *J. Chem. Phys.* **1986**, *85*, 636. *J. Phys. Chem.*, in press.

Molecular Dynamics Study of Chemical Reactivity in Liquid Sulfur

Frank H. Stillinger* and Thomas A. Weber

AT&T Bell Laboratories, Murray Hill, New Jersey 07974 (Received: December 2, 1986)

Molecular dynamics simulation employing 1000 atoms has been used to examine rapid chemical reactions in fluid sulfur at high temperature. A combination of two-atom and three-atom potentials has been used to represent interactions, with specific forms chosen to improve our earlier exploratory modeling for sulfur. The rate of loss of S_8 rings from media initially composed entirely of these molecules has been measured at 870, 1050, and 1310 °C. Spontaneous formation of large linear polymers has been observed. Initial stages of the reaction sequences exhibit a peculiar dominance of species containing even numbers of atoms, which appears to stem from bond alternations produced by the model along diradical chains. The artificial system with only three-atom potentials operative is proposed as a suitable "reference substance" for implementing a perturbation theory of liquid sulfur at equilibrium, and molecular dynamics has been used to obtain the corresponding pair correlation functions both before and after quenching to potential energy minima.

I. Introduction

When the molecular dynamics simulation technique was first applied to the study of condensed matter, attention focused for practical reasons on models with pairwise additive central atomic interactions.[1,2] Even so restricted, that early research activity produced important illuminating insights, particularly concerning the liquid states of the prototypical noble gases. Subsequent evolution of the computer and of computer simulation has permitted study of polyatomic and polar substances (such as carbon tetrachloride,[3] water,[4] and the alcohols.[5]) Pairwise additive potential models however have largely remained the norm; in those few cases where nonadditive three-body interactions have been included they usually have influenced structure and other properties as relatively weak perturbations.[6,7]

In order to model substances in which directed and saturable chemical bonds can form and break, pairwise additive potential functions are inappropriate. At a minimum, pair bonding in-

(1) Alder, B. J.; Wainwright, T. E. *J. Chem. Phys.* **1959**, *31*, 459.
(2) Rahman, A. *Phys. Rev.* **1964**, *136*, 405.

(3) McDonald, I. R.; Bounds, D. G.; Klein, M. L. *Mol. Phys.* **1982**, *45*, 521.
(4) Rahman, A.; Stillinger, F. H. *J. Chem. Phys.* **1971**, *55*, 3336.
(5) Jorgensen, W. L. *J. Am. Chem. Soc.* **1981**, *103*, 341, 345.
(6) Barker, J. A.; Bobetic, M. V. *J. Chem. Phys.* **1983**, *79*, 6306.
(7) Wojcik, M.; Clementi, E. *J. Chem. Phys.* **1986**, *84*, 5970.